DETERMINING THE ROLE OF NEGLECTED N^+ HEAVY IONS IN THE EARTH'S INNER MAGNETOSPHERE

BY

MEI-YUN LIN

THESIS

Submitted in partial fulfillment of the requirements
for the degree of Master of Science in Electrical and Computer Engineering
in the Graduate College of the
University of Illinois at Urbana-Champaign, 2019

Urbana, Illinois

Adviser:

Assistant Professor Raluca Ilie

ABSTRACT

Changes in the heavy ion composition in the Earth's terrestrial ionosphere and magnetosphere can have significant impacts on the particle dynamics in the Earth's magnetosphere-ionosphere system. The contribution of N^+ to the ring current population, in addition to that of O^+, has long been neglected, primarily because most instruments flying in space could not distinguish between O^+ and N^+ due to their similar masses. For example, the magnetospheric missions, such as the Magnetospheric Multiscale Mission and the Van Allen Probes, cannot distinguish N^+ from O^+ because of their similar masses. However, the limited observations of N^+ both in the ionosphere and magnetosphere indicate that N^+ in the Earth's magnetosphere and ionosphere is significant and a constant companion of O^+, especially during the storm time. Moreover, the variation of the N^+/O^+ ratio depends on the solar condition. In spite of only 12% mass difference, N^+ and O^+ have different charge exchange cross sections with geocorona neutral H, especially at higher particle energies. Since the charge exchange collision constitutes the dominant mechanism of the decay of the ring current during the slow recovery phase of a geomagnetic storm, tracking the respective behaviors of N^+ and O^+ ions in the inner magnetosphere is required. We have already modified the Hot Electron Ion Drift Integrator (HEIDI) model, the ring current model, to account for the motion of N^+ ions in the Earth's ring current. In order to assess the contribution of N^+ in the evolution of the ring current, we analyzed the behavior of N^+ in the ring current with HEIDI in a synthetic storm simulation. The simulation results show that the N^+ ions in the inner magnetosphere are lost at different rates than the energetic O^+ ions because of different charge exchange cross section. Moreover, the presence of N^+ in the ring current can impact the magnetospheric process, leading to a faster recovery rate of a geomagnetic storm.

To my parents, for their love and support.

ACKNOWLEDGMENTS

I would like to first thank to my adviser, Raluca Ilie, for her passion about research and patience in advising me. Without her support, I would not have had the chance to attend graduate school in the United States and step into the research on space science. I also would like to thank to Alex Glocer for his tremendous support with the development of the polar wind model. In addition, I sincerely appreciate my fellow colleagues, Jianghuai Liu, Yu Huang, Fraz Bashir, and Abdullah Khan for their precious suggestions, time and effort.

Permission is granted by the Center for Space Environment Modeling (CSEM) at the University of Michigan to use the SWMF and its module HEIDI for noncommercial education and research purposes. This project is funded by the Air Force Office of Scientific Research (AFOSR) and the National Science Foundation (NSF).

TABLE OF CONTENTS

CHAPTER 1

INTRODUCTION

1.1 Space Weather

Space weather is similar to the terrestrial tropospheric weather on the Earth, which features such events as wind and rainfall. Space weather involves geomagnetic storms and substorms. Both space weather and tropospheric weather start with the Sun. A small amount of the radiation and energy from the Sun can dramatically change the behavior of space weather, as well as the tropospheric weather.

According to the United States National Space Weather Program, space weather refers to weather conditions between the Sun, the solar wind and the Earth's atmosphere. During a geomagnetic storm, the magnetic field of the Earth can rapidly change. Figure 1.1 shows the influence of space weather on the Earth.

Intense geomagnetically induced currents (GIC) are generated in the Earth's atmosphere during the large geomagnetic storms, due to the large variation of the Earth's magnetic field. The GICs are especially strong in high-latitude regions such as Canada and Finland. Oil and gas pipelines, electrical power transmission grids, and communication systems are all susceptible to the GICs. In addition, the operation and performance of the satellites and the ground-based technological systems can be disrupted by the severe space weather conditions. Energetic particles in the Earth's ionosphere and magnetosphere can penetrate the protective shells of the spacecraft and accumulate inside the spacecraft. The accumulation of charges can cause damage to the on-board electronics and the instruments [1]. It is estimated that trillions of dollars, on the order of the gross domestic product of a large country, will be

lost immediately after an extreme space weather event happens on the Earth [2].

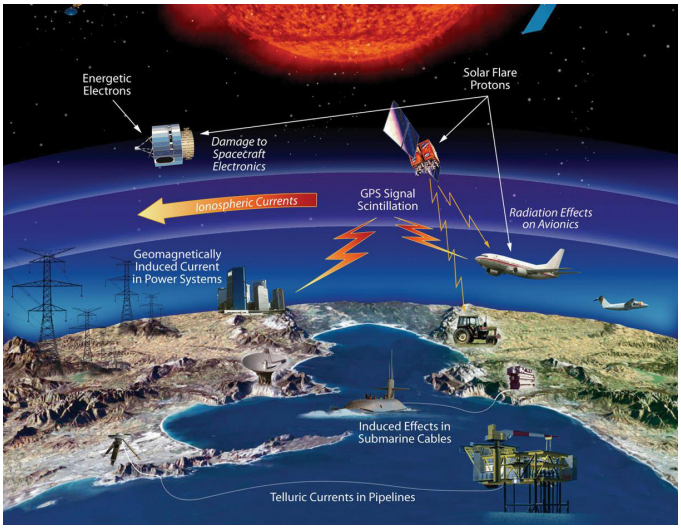

Figure 1.1: Space weather impact on the Earth (credit: NASA [3]).

.

1.2 Global Magnetosphere

The Earth has an internal dipole magnetic moment, attributed to the dynamo of the electrically conducting fluid inside the core of the Earth [4]. On the surface of the Earth, the magnitude of the Earth's magnetic field is around 36,000 nT. The magnitude of perturbation in magnetic field is not large (only a few tens of nT); however, the rapid change of the Earth's magnetic field can cause severe problems.

The Earth's global magnetosphere is defined as the region where the Earth's magnetic field dominates. Inside the Earth's magnetosphere, the plasma and the electromagnetic fields are controlled by the Earth itself, while outside the magnetosphere they are dominated by the external sources, such as the solar wind, an ionized thermal plasma flowing out from the Sun. The magnetospheric fluids consist of energetic ions, and cold and hot plasma, all of which contribute to the magnetospheric dynamics [5]. Different regions are governed by different physical regimes. The magnetosphere contains several

large-scale regions, which vary in terms of the composition, energies, and densities of the plasma.

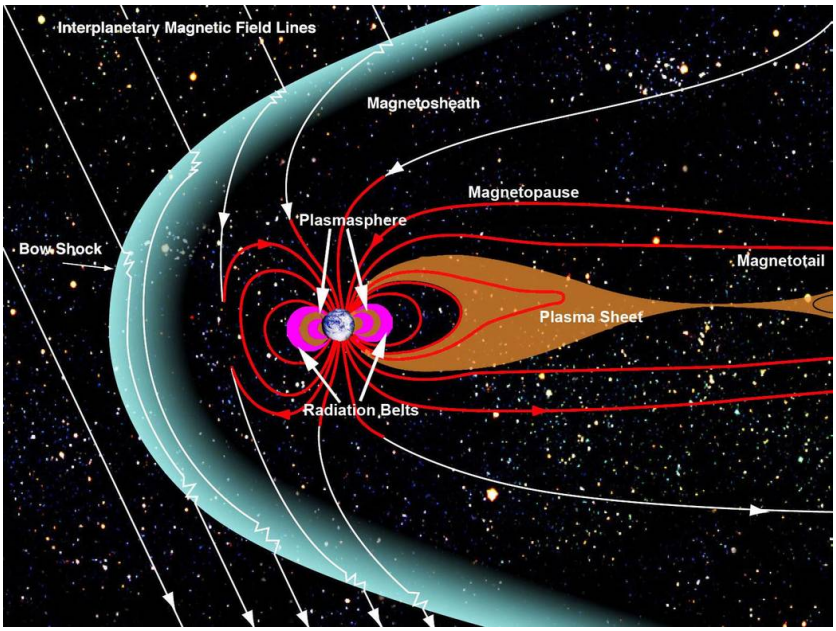

Figure 1.2: Illustration of the Earth's magnetosphere (credit: NASA [6]).

.

The Earth's magnetospheric dynamics is due to interplay between the interplanetary magnetic field (IMF) and the geomagnetic field itself. When the solar wind impedes on Earth, as shown in Figure 1.2, these fast moving, high energy, and magnetized solar wind particles cannot penetrate the Earth's magnetosphere directly. Therefore, the magnetospheric cavity is formed. In the front of the magnetospheric cavity, a bow shock can slow down the solar wind and the solar wind plasma starts to flow around the Earth's magnetosphere. The solar wind plasma speeds up again when it approaches the magnetopause, a boundary between the solar wind plasma and the Earth's magnetosphere. The flowing solar wind particles then start to compress the dayside magnetosphere and stretch out the nightside magnetosphere. After the nightside reconnection happens, there is an injection that brings the energetic particles from the plasma sheet, a hot and dense plasma extending along the magnetotail, back to the inner magnetosphere.

The magnetopause location is defined as the region where the dynamic pressure p from the solar wind equals the magnetic pressure inside the Earth's magnetosphere p_B (see Equation 1.1).

$$p_B = \frac{B^2}{2\mu_0} = \rho_{sw} u_{sw}^2 = p \tag{1.1}$$

where $\mu_0 = 4\pi \cdot 10^{-7}$ is the permeability of free space, B represents the magnetic field of the magnetopause, ρ_{sw} is the mass density of the solar wind and u_{sw} is the solar wind flow speed. The nose of the magnetopause is located about 10 R_E away from the Earth on average [7].

There are three particle populations inside the inner magnetosphere: the Van Allen radiation belts, the ring current ions and the plasmasphere. The plasmasphere consists of cold ions with energies below 10 eV. The ions in the plasmasphere mostly come from the Earth's ionosphere and they usually corotate with the Earth. The population of ring current ions and Van Allen radiation belt ions are high energy particles, such that they obey the cyclotron motion along the Earth's magnetic field lines and bounce back and forth between the northern and southern hemisphere. In addition to those two drifts, they also slowly drift around the Earth due to the gradients and curvature of the geomagnetic field. The ring current ions mainly consist of O^+, H^+, He^+ and possibly, N^+, with energies between 1 keV and 200 keV, while the radiation belt ions are mostly protons and electrons with energies over 200 keV.

1.3 Ring Current

The ring current is a toroidal shaped current formed by the gradient curvature drift of the trapped particle ions in the Earth's magnetic field. It consists of ions whose energies vary from 1 keV to 200 keV and drift around the Earth. The ring current ions are usually located from 2 to 9 Earth radii. The ring current dominates the energy density of the inner magnetosphere, and its intensification is highly associated with the geomagnetic storm conditions [8, 9].

1.3.1 The Transport of the Ring Current Ions

The ring current particles are trapped by the Earth's magnetic field and perform three types of motion [10]. The first one is the gyro-motion around a magnetic field line. The gyro-radius (r_c) performed by the charged particles is defined as Equation 1.2.

$$r_c = \frac{v_\perp}{\Omega_c} = \frac{mv_\perp}{|q|B} \tag{1.2}$$

where $v_\perp$ is the velocity perpendicular to a magnetic field line, Ω_c is the gyro-frequency, q represents the charge of the particle and B is the magnitude of a magnetic field.

The second motion is the bounce motion where charged particles bounce back and forth along the magnetic field lines. Because the second motion assumes the conservation of magnetic moment (μ_m), charged particles encounter difficulty in moving toward the stronger magnetic fields, and therefore become trapped by the geomagnetic field. The third motion is the gradient-curvature drift, due to the magnetic field spatial variation, both in magnitude and direction. The drift gradient curvature drift velocity is expressed as Equation 1.3.

$$v_{GC} = \frac{m}{q}\frac{v_\parallel + \frac{1}{2}v_\perp^2}{B_0}\frac{B_0 \times \bigtriangledown B_0}{B_0^2} \tag{1.3}$$

where m and q represent the mass and charge of the particles, $v_\parallel$ and $v_\perp$ are the velocity parallel and perpendicular to the magnetic field lines, respectively. Equation 1.3 indicates that the drift velocity depends on the gradient of magnetic field, and ions and electrons drift in different directions around the magnetic cavity. These three motions are described by different adiabatic invariants, and the combination of three motions represents the motion of the ring current ions in the Earth's magnetic field. Figure 1.3 represents the superposition of these three motions that a charged particle undergoes under the influence of the Earth's magnetic field.

1.3.2 The Source of the Ring Current Ions

During the quiet time, the ring current tends to be symmetric, and it is composed of a low number density of ions. However, during geomagnetically

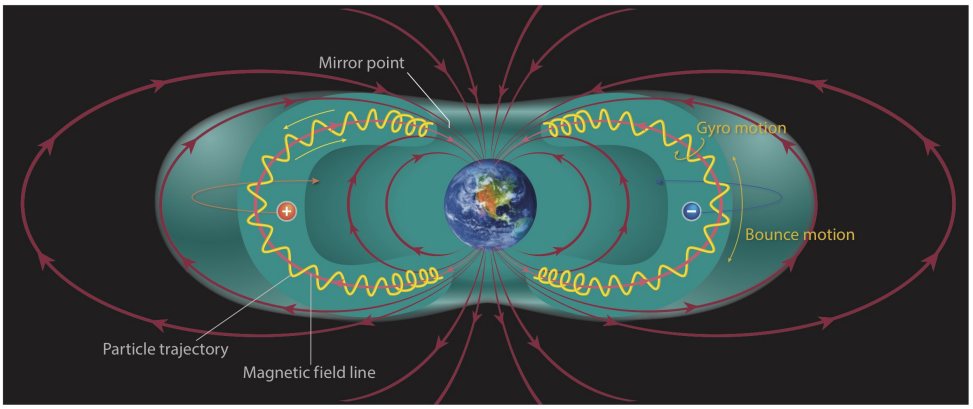

Figure 1.3: Illustration of the charged particle motion trapped in the Earth's magnetic field.

.

active times, ions are accelerated and injected from the plasma sheet into the Earth's inner magnetosphere. This is a time when the ring current starts to intensify and becomes asymmetric.

The main carriers of the storm ring current are energetic O^+, H^+, He^+, N^+ and electrons. Heavy ions such as O^+ and N^+ must come from the Earth's ionosphere, and light ions like H^+ originate both in the solar wind or the Earth's ionosphere. The ion composition of the ring current ions is largely affected by the size of the geomagnetic storm [9]. During the severe geomagnetic storms, the composition of the ring current can be dominated by heavy ions. The existence of heavy ions in the ring current is significant and the energy density of the ring current mostly depends on the heavy ions distribution. The electrons, on the other hand, contribute little to the energy density due to negligible masses.

1.3.3 The Decay of the Ring Current

The decay of the ring current leads to the recovery phase of the geomagnetic storms and the restoration of magnetospheric dynamics back to pre-storm state. Different loss mechanism occur during different stages of a geomagnetic storm.

The main loss mechanism of the ring current ions are the charge exchange collisions, the flow-out to the dayside magnetosphere, the wave-particle interactions, the Coulomb collisions, and the particle precipitation.

The charge exchange collisions of ring current ions with the neutral hydrogens from the geocorona are the dominant loss mechanisms for the decay of the ring current during the slow recovery phase of a geomagnetic storm [11]. Energetic ions are originally bounded to the Earth's magnetic field. The geocorona is an extension of the exosphere to several Earth radii and consists of cold and dense neutral hydrogen atoms. The probability of charge exchange reactions depends on the the charge exchange cross section, the number density of the geocorona neutral hydrogen, and the energy of the ring current ions. When a ring current ion exchanges an electron with a neutral atom, the neutral becomes the energetic neutral atoms (ENA), which are not affected by the magnetic field.

While the charge exchange collision constitutes the main loss mechanisms of the ring current decay in the slow recovery phase of a geomagnetic storm, the flow-out to the dayside magnetosphere is the dominant mechanisms of the loss of the ring current during the main phase and the early recovery phase of a geomagnetic storm. During the storm time, ring current ions drift from the nightside magnetosphere to the dayside magnetosphere, forming an asymmetric ring current. As they drift around the Earth, most of the ring current ions flow out on open drift paths [12, 13]. Because of the large fraction of the flow-out ring current ions, the asymmetric ring current gradually becomes symmetric, leading to the recovery phase of a geomagnetic storm.

Coulomb collisions mostly affect the low-energy ring current ions [14]. An energetic charged particle collides with the thermal electrons or ions, causing the change of the pitch angle of a charged particle. In addition, the wave-particle interaction occurs when the frequency of the electromagnetic (EM) wave is similar to the cyclotron frequency of a charged particle. The resonance between the EM wave and a charged particle is then constructed, and therefore the energy transfer between the wave and charged particles causes the loss of the ring current [15].

1.4 Geomagnetic Indices: The Dst and Kp Index

We introduce here two of the geomagnetic indices we use most in the analysis of geomagnetic storms: the disturbance storm time (Dst) index and the Kp index.

The Dst index is derived by the averaging disturbance of $B_{\parallel}$ near the Earth's equator, as it is based on data from four ground-based magnetometers in the low-latitude regions. Therefore, the Dst index provides a proxy for the strength of the ring current. The time scale of the Dst index is one hour. Generally, an intense geomagnetic storm is defined by Dst index that is smaller than -100 nT, and an extreme storm is defined by the minimum Dst index less than -250 nT.

The Kp index also depends on the fluctuation in the geomagnetic field. The index range is from 0 to 9. An intense geomagnetic storm is typically defined as a Kp index over 7. The time scale of the Kp index is 3 hours and it is based on data from 13 ground-based magnetometer stations around mid-latitudes. The German Research Centre for Geosciences (GFZ) in Potsdam, Germany, finalizes and stores the Kp index. The Kp index is largely used by the Space Weather Prediction Center to announce the space weather warnings.

1.5 Geomagnetic Storms

Space weather starts at the Sun, which can generate hot and energetic plasma from its atmosphere and eject it into space in what is called a coronal mass ejection (CME). A CME will travel through space and can reach the Earth, and the energy of a CME is sufficient to affect the Earth's intrinsic magnetic field causing a geomagnetic storm. There are three phases in a geomagnetic storm: the initial phase, the main phase and the recovery phase.

The first stage is the initial phase, when an abrupt increase of the Earth's magnetic field happens. During the initial phase, the dayside magnetosphere is compressed and the magnetopause current starts to increase, leading to an increase in the geomagnetic field, which corresponds to a rise in the Dst

index identified as the storm sudden commencement (SSC) (shown in Figure 1.4). The SSC marks the beginning of a geomagnetic storm.

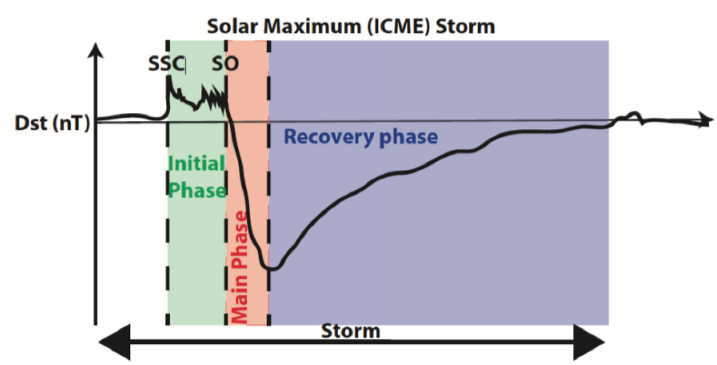

Figure 1.4: The evolution of the Dst index in a geomagnetic storm.

.

The second stage is the main phase, during which charged particles from the plasma sheet are being injected into the near Earth region. At this stage, the ring current starts to intensify and the flow-out to the dayside magnetosphere is the main loss mechanism of the ring current particles. During the main phase, the main feature of the Dst index is the depression of geomagnetic field. For an intense geomagnetic storm, we can expect Dst index to reach -100 nT or lower during the main phase.

When the convection subsides, the third stage, known as the recovery phase of a geomagnetic storm, begins. The whole magnetospheric dynamics and the Dst index begin to recover back to the pre-storm state. In the early stage of the recovery phase, the main loss mechanism of the ring current is still the flow-out to the dayside magnetosphere. However, other loss mechanisms, such as Coulomb collision, wave-particle interaction and charge exchange collisions, start to play a role in the decay of the ring current. During the slow recovery phase of a geomagnetic storm, charge exchange collision becomes the dominant loss mechanism in the decay of the ring current.

1.6 Space Weather Modeling

The Sun-Earth system is a time-dependent, three-dimensional, multi-component and complex natural system. There are multiple interconnecting elements inside the Sun-Earth system, involving transfer of mass, momentum, energy and heat. Because these nonlinear physical processes cannot be analytically assessed, modeling the space weather numerically helps us understand the system-wide response to the space weather and predict the impact of space weather on the Earth.

Modeling space weather is a difficult challenge due to the complexity of the space environment. Different phenomena pertaining to space weather are governed by different physical processes, and the temporal and spatial scales are all different. Space weather models are mathematical tools used to simulate the space environment of the Sun-Earth system. Current space weather modeling techniques usually fall into the following categories: (1) first principles modeling, which uses mathematical equations to model physical processes, (2) empirical modeling, which is based on the observation data, (3) semi-empirical modeling, which ranges from complex physics based modeling augmented by data assimilation, to simple linear fits to data.

1.6.1 Space Weather Modeling Framework (SWMF)

The SWMF is a robust, high-performance space weather modelling system that describes the physics of the Sun-Earth system. There are 12 components currently in the SWMF: (1) solar corona (SC), (2) eruptive event generator (EE), (3) inner heliosphere (IH), (4) solar energetic particles (SP), (5) global magnetosphere (GM), (6) inner magnetosphere (IM), (7) radiation belt (RB), (8) ionosphere electrodynamics (IE), (9) upper atmosphere (UA), (10) lower corona (LC), (11) outer heliosphere (OH) and (12) polar wind (PW). The various SWMF components are based on first principles methods, but some of the models are applied with the participation of empirical models to simplify the computations. Each domain can run as a stand-alone model, but they can be coupled with each other to represent the system-wide response of the Sun-Earth system. The coupling between each element in the SWMF is shown in Figure 1.5.

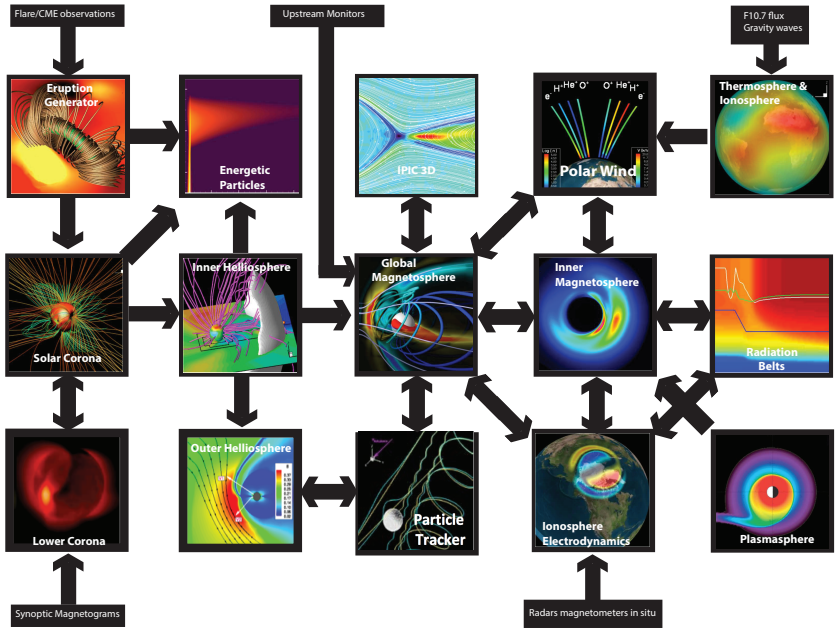

Figure 1.5: The various SWMF components. Arrows indicate coupling between models.

.

CHAPTER 2

DETERMINING THE ROLE OF N^+ IN THE EVOLUTION OF THE RING CURRENT

2.1 Motivation: Observation of N^+ in the Magnetosphere and Ionosphere

Ion composition of the magnetospheric plasma significantly affects the magnetospheric dynamics. It has been reported that heavy ions, which most studies considered to be O^+ only, control the mass and energy flow in the Earth's magnetosphere [9, 16, 17]. Therefore, the presence of N^+ can further impact the dominating physical mechanisms that dictate the dynamics in the near Earth region.

Studies based on data from the Charge Composition Explorer (CCE) instrument on board the Active Magnetospheric Particle Tracer Explorer (AMPTE) spacecraft [18] showed that in the Earth's magnetosphere, high-energy N^+ are the third most abundant ion species during storm time. Even during the quiet time, fluxes of high-energy O^+ and N^+ are compatible (see Figure 2.1). In addition, observations from the WIND spacecraft showed that the solar cycle can affect the N^+/O^+ ratio. Data from the WIND spacecraft indicates that high N^+/O^+ ratio, varying from 0.45 to 0.6, occurs in the nightside magnetosphere during solar minimum, while low N^+/O^+ ratios ($\sim$0.25) occur during solar maximum [19] (see Figure 2.2). These limited observations in the Earth's magnetosphere confirm that the contribution of N^+ in the Earth's magnetosphere is significant, and the variation of N^+/O^+ depends on solar cycle.

The presence of N^+ in the magnetosphere indicates that it must be of ionospheric origin. The transport and acceleration mechanisms of heavy ions in the ionospheric outflow have been studied for a long time, since the classical

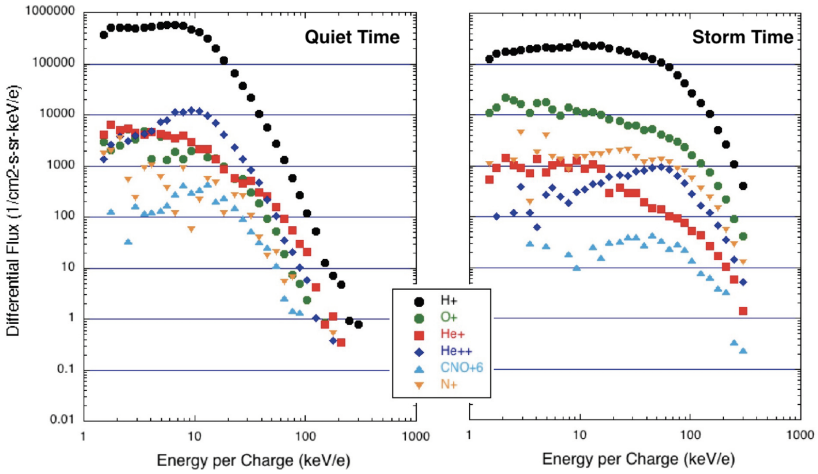

Figure 2.1: AMPTE measurements showing differential ion fluxes vs. energy per charge (courtesy of Lynn Kistler).

.

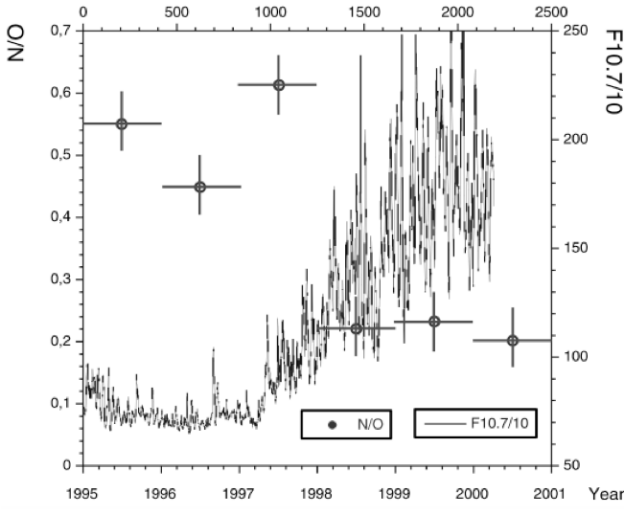

Figure 2.2: Measured N^+/O^+ and F10.7 between 1995 – 2001 [19].

.

polar wind theory is insufficient to explain the acceleration of the heavy ions in the ionospheric outflow. In fact, there has been much interest in the transport and acceleration of ionospheric O^+ since it was first reported by [20]. Since then, the contribution of ionospheric O^+ outflow in the magnetospheric dynamics has been amply studied [9, 21–26]. Nevertheless, the contribution of N^+ in the polar wind outflow has not been explained thoroughly, and the kinetic mechanisms behind the outflowing N^+ are still unknown. Early NASA observations have pointed out the presence and importance of N^+ in

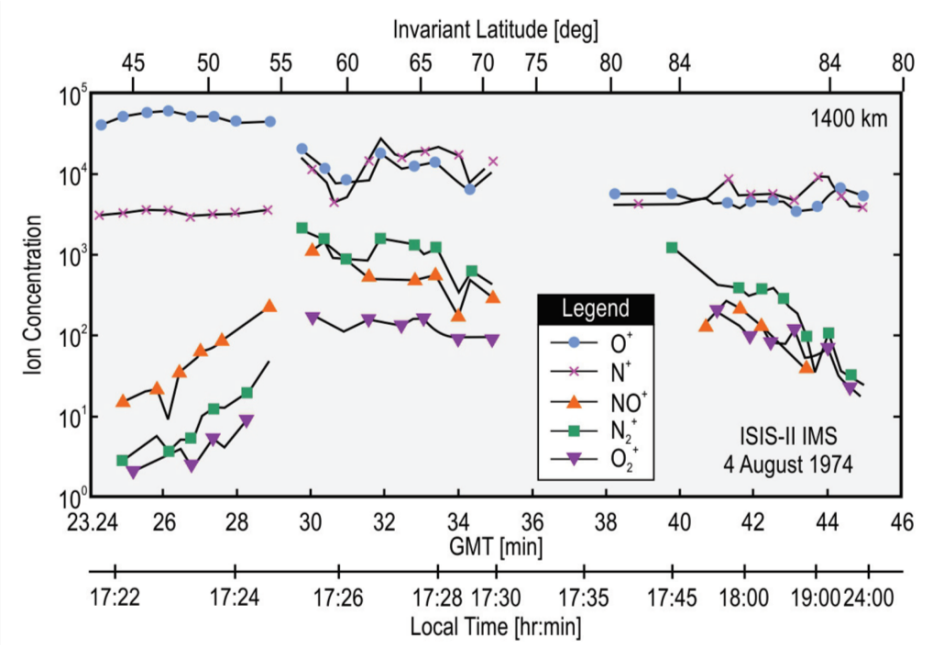

Figure 2.3: ISIS 2 measurements of ion composition during the August 1972 storm showing increased N^+ (red), O^+ (blue) and molecular ions species abundances at 1400 km. Figure adapted from Hoffman et al. [27].

the ionosphere. Figure 2.3 shows the data from ISIS 2 IMS observations during the 4 August 1972 storm (Kp=9) [27]. During this geomagnetically active time, which starts around Local Time 17:25, O^+ and N^+ have comparable concentrations from 55 latitude to the pole at 1400 km altitude. Moreover, during the main phase of this storm, molecular ions such as NO^+, N_2^+ and O_2^+ have large concentrations ($\sim 10^3$ cm^{-3}) as these observations show.

Chappell et al. [28] successfully separated the N^+ and O^+ species, and RIMS measurements suggested that N^+ is a constant companion of outflowing O^+ during the storm time [29]. Observation data from the Superthermal Mass Spectrometer (SMS) on board the Akebono satellite ([30, 31]) confirmed the presence of N^+ in the ionosphere and showed that the ratio of N^+/O^+ can be around unity in the dayside high-altitude (> 1000 km) polar (> 70) ionosphere during the main phase of large storms. Furthermore, Akebono SMS measurements indicated that during storm time, the relative abundance of N^+ increases dramatically, and at some times N^+ can be the dominant ion in the high-latitude ionosphere. Figure 2.4 shows ion flux measurements during the 12-13 March 1990 storm (Kp=7+) from the SMS instrument on board

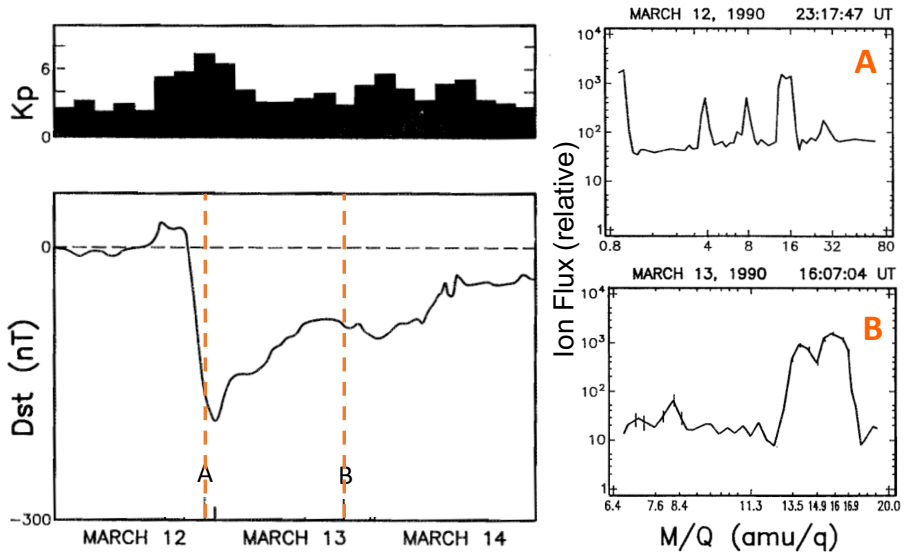

Figure 2.4: Selected SMS mass spectra in the storm time during 12-13 March 1990 show the ion abundance of O^{++} (8 AMU q^{-1}) and N^{+} (14 AMU q^{-1}). Panel A is observed during the main phase of the storm and Panel B is observed during the recovery phase of the geomagnetic storm [31].

the Akebono satellite confirming the presence of N^{+} in the high-latitude ionosphere. The Akebono SMS instrument also demonstrated that the thermal ion population, for which energies are below 30 keV, in the high-altitude polar ionosphere can be composed of H^{+}, N^{+}, He^{+}, O^{+} and O_2^{+} [32]. Although these observations of N^{+} show the importance of N^{+} in the high-latitude ionosphere, the mechanisms responsible for accelerating the ionospheric N^{+} from eV to keV energies are still largely unknown. The transport and acceleration of N^{+} in the ionospheric outflow, as well as the relative abundance of N^{+} in comparison with O^{+}, needs further exploration.

2.2 Scientific Importance

The ion composition of the magnetospheric plasma can alter the magnetospheric dynamics, the ring current formation and decay, and the mass loading of magnetospheric plasma. In addition, the ion composition of the Earth's magnetosphere can greatly affect wave properties and propagation. The existence of N^{+} in the global magnetosphere can change the dispersion relation in

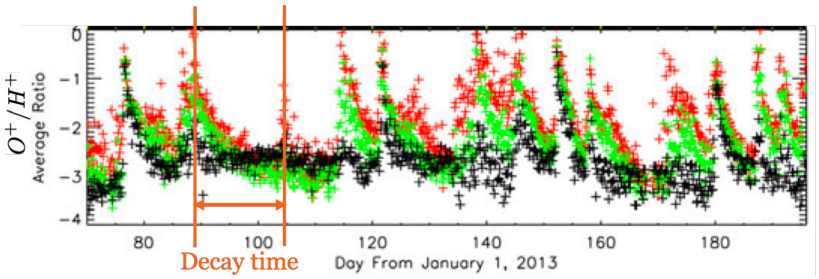

Figure 2.5: RBSPICE measurements of average ratio O^+/H^+ in three L shell bins; black for L = 3–4, green for L = 4–5, and red for L = 5–6 [34].

.

electromagnetic ion cyclotron (EMIC) waves [33]. The presence of N^+ in the magnetosphere also plays a crucial role in the analysis of data from current magnetospheric missions, such as the Van Allen Probe and Magnetospheric Multiscale Spacecraft (MMS). These missions consider heavy ions as belonging to the carbon-nitrogen-oxygen (CNO) group, which means they consider the mass close to O^+ as the same species. This might include contributions of N^+ into O^+, since the mass resolutions in the Van Allen Probe and the MMS are insufficient to separate N^+ from O^+. For instance, the Radiation Belt Storm Probe Ion Composition Experiment (RBSPICE) instrument on the Van Allen Probe reported unexplained observations of the fast decay of O^+ at large L shells [34]. In Figure 2.5, the orange line marks the time when the ratio of O^+/H^+ approaches the maximum and when the ratio of O^+/H^+ becomes the minimum. Figure 2.5 indicates that the decay times of the O^+/H^+ ratios in large L shell and small L shell are similar, which seems counter-intuitive. The presence of the fast-decaying N^+ in the magnetospheric plasma might explain such fast decays, since N^+ has a shorter lifetime in the magnetosphere than O^+.

Overall, determining the role of N^+ in the evolution of ring current enhances our understanding of plasma transport processes throughout the magnetosphere, and thus helps the interpretation of observations from various magnetospheric missions.

2.3 Difference of N^+ and O^+ in the Ring Current

The overarching objective of this thesis is to determine the role of N^+ in Earth's inner magnetosphere dynamics. The importance of O^+ in the Earth's magnetosphere-ionosphere system has been the subject of numerous studies [e.g. 9, 11, 22, 25, 35], but only a few studies reported on the importance of N^+. Previous research considered heavy ions such as O^+. This was due to the small 12% difference in atomic mass between N^+ and O^+, as well as the same electric charge. However, N^+ and O^+ have different properties, such as charge exchange cross section, ionization energies, and scale heights. Charge exchange collisions constitute the main loss mechanism for ring current ions during the slow recovery phase of a geomagnetic storm. Energetic ions are bounded to the Earth's magnetic field and through the process of charge exchange, they transfer an e^- to a neutral atom and become energetic neutral atoms (ENAs).

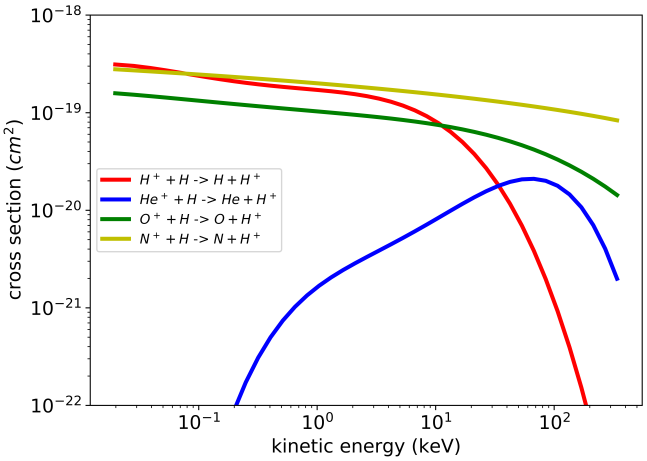

Figure 2.6: Cross section for charge exchange reactions between ring current ions and exospheric neutral hydrogen.

Then, the newly formed ENA is suddenly unaffected by the ambient magnetic field. Therefore, charge exchange collisions between hot ring current ions (H^+, O^+, He^+ and N^+) and neutral exosphere atoms can remove ions trapped in geomagnetic field, causing loss of the ring current population, and hence the decay of the ring current. The charge exchange lifetime is highly dependent on charge exchange cross section, which in turn depends on the

energy of the ion species, and the abundance of neutral hydrogen atoms in the exosphere. Figure 2.6 shows that at high energies (>12 keV), the difference in charge exchange cross section for reactions O^+ and N^+ with neutral hydrogen becomes significant (e.g. for a 20 keV particle, the difference can be 50%). The reaction between energetic N^+ and neutral hydrogen has a relatively large charge exchange cross section. Therefore, N^+ is more likely than O^+ to transfer an electron to the ambient neutral hydrogen. The different collision possibilities imply that N^+ and O^+ can have different trajectories, and hence different pathways of energization, in the Earth's magnetosphere.

2.4 Method: Ring Current Modeling

Numerous ring current studies have already indicated that the ring current plays a crucial role in the depressions of the Dst index [9, 36–38]. Global magnetosphere models, such as BATS-R-US, solve the MHD equations and treat the plasma as a fluid with embedded magnetic field, but do not accurately describe kinetic effects. On the other hand, ring current models focus on solving the kinetic equations of energetic charged particles, but lack the accurate representation of time-varying electromagnetic fields. The global MHD magnetosphere model itself lacks the ability to include the kinetic description of the ring current and thus oversimplifies the behavior of the magnetosphere. Multiple studies addressed the importance of including a ring current model in the geomagnetic storm simulations [39–42].

Glocer et al. [25] pointed out that the simulated Dst index is also largely affected by the inclusion of relevant kinetic physics via coupling of the MHD solution with the solution provided by a ring current model. Not including a ring current model in the geomagnetic storm simulations can lead to inaccurate representation of the magnetosphere current system. Therefore, the development of the ring current models, and their inclusion and coupling with global magnetospheric models, is essential in order to completely model the whole magnetosphere-ionosphere system.

In this work, we analyze the contribution of nitrogen ions to the overall plasma dynamics in the inner magnetosphere, by operating the Hot Electron

Ion Drift Integrator (HEIDI) ring current model under the Space Weather Modeling Framework (SWMF). We properly include the contribution of N^+ ions in the ring current model and assess the role of outflowing N^+ ions in the overall inner magnetosphere dynamics. Here, we further develop the modified five species (H^+, He^+, O^+, N^+ and e^-) of HEIDI to account for the contribution of N^+ to the ring current.

2.4.1 Hot Electron Ion Drift Integrator (HEIDI)

HEIDI is part of the inner magnetosphere subsystem of the SWMF, and it is a kinetic drift model of the ring current, solving the time-dependent, gyration- and bounce-averaged Boltzmann equation [43].

$$\frac{\partial Q}{\partial t} + \frac{1}{R_0^2}\frac{\partial}{\partial R_0}(R_0^2\langle\frac{dR_0}{dt}\rangle Q) + \frac{\partial}{\partial \phi}(\langle\frac{d\phi}{dt}\rangle Q) + \frac{1}{\sqrt{E}}\frac{\partial}{\partial E}(\sqrt{E}\langle\frac{dE}{dt}\rangle Q) + \frac{1}{h(\mu_0)\mu_0}\frac{\partial}{\partial \mu_0}(h(\mu_0)\mu_0\langle\frac{d\mu_0}{dt}\rangle Q) = \langle\frac{\delta Q}{\delta t}\rangle_{collisions} \tag{2.1}$$

The kinetic equation solves for the phase-space distribution function $Q(R_o,\phi,E,\mu_o,t)$ for all pitch angles and local times on an equatorial plane, defined by the minimum of local magnetic field. R_0 denotes the geocentric distance in the equatorial plane, ϕ is the magnetic local time, and E stands for kinetic energy. The term $\mu_o = \cos\alpha$, where α represents the equatorial pitch angle, and t represents the time. The bracket $\langle\rangle$ indicates the bounce average of a certain quantity (see Equation 2.2), and the bounce average formalism is valid under the assumption of a slowly varying magnetic field.

$$\langle\rangle = \frac{1}{S_B}\int_{(s_{m'})_{s_m}} \frac{ds}{\sqrt{1-\frac{B(s)}{B_m}}} \tag{2.2}$$

where $B(s)$ is the magnetic field along the field line, s is the distance from the foot point of the magnetic field line and B_m is the magnitude of the magnetic field at the mirror point. The terms s_m and $s_{m'}$ are two of the mirror points along a magnetic field line and S_B represents the half-bounce path length. Since the ring current drifts in the equatorial plane, HEIDI defines the equatorial plane as the plane of minimum magnetic field.

HEIDI can accommodate arbitrary magnetic field [43]. Arbitrary magnetic field can represent the magnetic field during the storm time, when the magnetic field of the Earth is no longer a magnetic dipole and the equatorial plane is therefore not a flat plane. In order to accommodate this feature, HEIDI uses α as a stretched factor, which can compress the dayside magnetic field and stretch out the nightside magnetic field. In addition, HEIDI incorporates empirical models for the electric field, such as the Weimer model and the Volland-Stern two-cell convection pattern [44–46].

HEIDI originally accounted for four ring current ion species, which are H^+, He^+, O^+ and e^-, and we have modified the HEIDI model to include the contribution of N^+ to the ring current. The particle energy typically ranges from 10eV to 400 keV and L shell values from 2 to 6.5 R_E. The term $\frac{\delta Q}{\delta t}_{collisions}$ in Equation 2.1 represents the changes of distribution functions due to the losses of the ring current. It can account for the loss of the ring current due to flow-out of plasma to the dayside magnetopause, Coulomb collision with the thermal plasma, particle precipitation, and charge exchange loss with the geocoronal hydrogen.

2.4.2 Geocorona Models

The probability of charge exchange of ring current ions and exospheric neutrals depends on the abundance of neutral atoms in the geocorona, which acts as an energy sink for ring current ions. HEIDI is the only ring current model to date that incorporates six geocoronal models. The six models, which are Rairden et al. [47], Hodges [48], Østgaard et al. [49], Zoennchen et al. [50], and Bailey and Gruntman [51, 52], predict different distributions of exospheric neutral density. Figure 2.7 shows the geocoronal distribution in equatorial plane with different geocoronal models. For instance, the Rairden et al. [47] model assumes a spherically symmetric exosphere based on the Dynamics Explorer 1 data, while the Hodges et al. [48] model, based on the Monte Carlo simulations, predicts a distribution of neutral H densities with day-night and dawn-dusk asymmetry. Developed from measurements by the Geocoronal Imager (GEO), the Østgaard et al. [49] model predicts asymmetric exosphere with higher densities on the nightside. Based on the TWINS

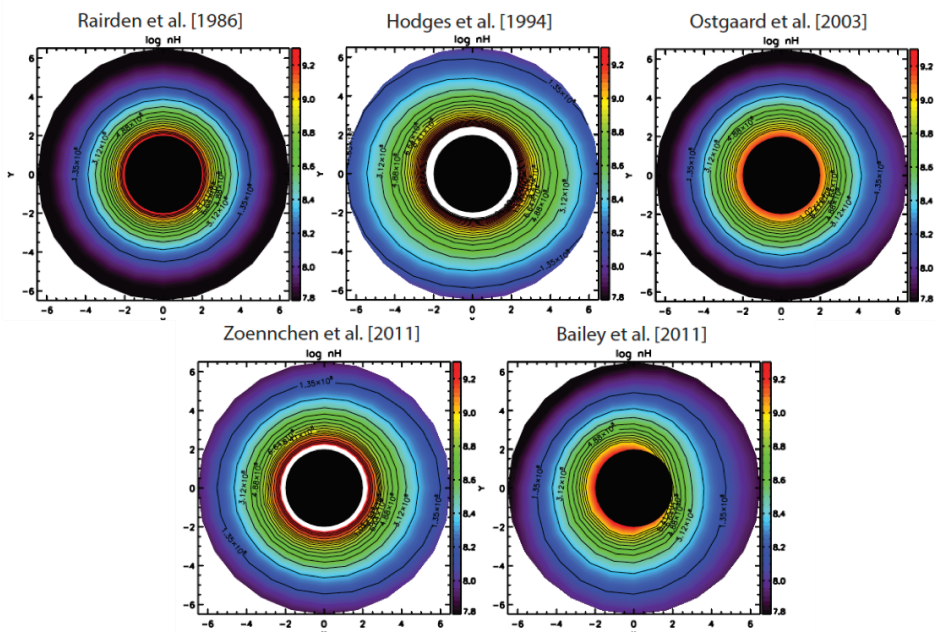

Figure 2.7: The top row presents the equatorial profiles for the geocoronal distribution as predicted by Rairden et al. (1986), Hodges (1994), and Østgaard et al. (2003) from left to right. The bottom row presents the geocoronal distribution of Zoennchen et al. (2011) and Bailey and Gruntman (2011).

Lyman-alpha Detector (LAD) observations, the Zoennchen et al. [50] model allows for longitudinally symmetric exosphere with day-night asymmetries, and the Bailey and Gruntman [51] model shows dawn-dusk and day-night asymmetric exosphere. In addition, the Bailey and Gruntman [52] model, also derived from the TWINS LAD data, predicts a geocoronal density distribution that depends on solar activity. With the numerical capabilities of the HEIDI, we can examine how neutral dynamics influence the loss of ring current heavy ions, by testing the influence of various geocoronal models on the development and decay of ring current, while taking into account the contribution of nitrogen ions to the overall plasma composition.

2.4.3 HEIDI Idealized Simulation

To run the HEIDI model, we need to specify several parameters, including the solar wind conditions, boundary conditions, electric and magnetic field, and geocoronal models. This information can be assigned in the parameter files of HEIDI (see Figure 2.8). Then, HEIDI solves for the time evolution

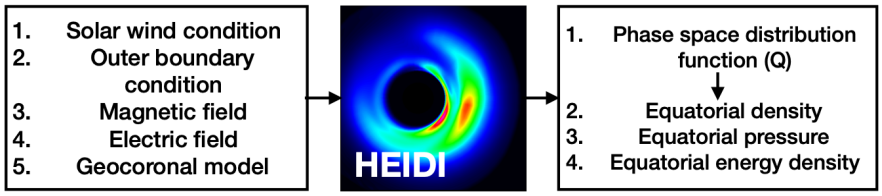

Figure 2.8: The input and output HEIDI needs for simulation. The left-hand side is the input of HEIDI and the right-hand side represents the output of HEIDI.

of the phase space distribution function (Q_s) via the Boltzmann equation, and thus calculates the equatorial density (Equation 2.3), pressure (Equation 2.4) and energy density (Equation 2.5).

$$n_s(r,t) = \int d^3 v_s Q_s(r, v_s, t) \tag{2.3}$$

$$P_s(r,t) = \int d^3 v_s m_s Q_s(r, v_s, t)(v_s - u_s)(v_s - u_s) \tag{2.4}$$

$$E_s(r,t) = \int d^3 v_s \frac{1}{2} m v_s^2 Q_s(r, v_s, t) \tag{2.5}$$

We have conducted numerical simulations using the newly developed HEIDI model, which includes the contribution from the nitrogen ions.

$$n_{heavy} = 0.011 exp[0.24K_p + 0.011F_{10.7}] \pm 0.16 \tag{2.6}$$

In this simulation, we assume that plasma parameters on the outer boundary are constant ($n_{heavy} = n_{O^+} + n_{N^+}$), and heavy ions densities on the outer boundary are set by the Young's formula in Equation 2.6 [53], which only provides the density of O^+ as a function of Kp and F10.7, and implies that the plasma composition changes on a timescale of 3 hours. We apply different N^+/O^+ ratios to assess the impact of N^+ on the magnetospheric dynamics. The range of the N^+/O^+ ratio varies from 0 to 1, which represents the percentage of N^+ in the ring current. For example, if the N^+/O^+ ratio is 0.1, this means we have 10% N^+ with 90% O^+. For simplicity, we used the neutral hydrogen model by the Rairden et al. [47] model, which assumes a spherically symmetric neutral hydrogen density distribution, and that of the Hodges [48] model, which predicts neutral hydrogen density distribution with day-night and dawn-dusk asymmetry.

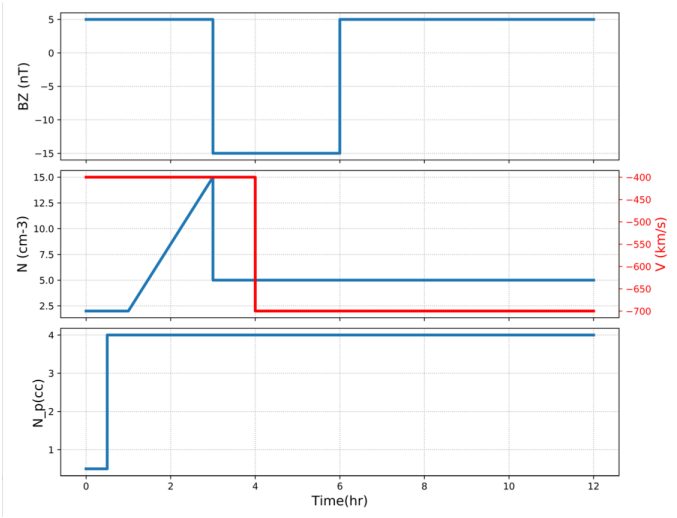

Figure 2.9: Synthetic solar wind condition for simulation. The top two rows are solar wind condition and the bottom row is MPA data for outer boundary condition.

Figure 2.9 shows the synthetic solar wind conditions, which mimic a geomagnetic storm in a 12 hour simulation. Top panel shows the interplanetary magnetic field Bz which changes polarity after 3 hours, remains at -15 nT, and after another 3 hours, turns back to the initial value and remains constant. This behavior implies that the decay of the ring current starts in the sixth hour. The density of the outer boundary is low for the first 30 mins, and then increases to 4 cm^{-3}. In the Chapter 3 we discuss in detail the results of the first ring current simulation which includes the contribution of nitrogen ions to the magnetospheric plasma.

CHAPTER 3

RESULTS AND DISCUSSION

Charge exchange is the dominant loss mechanism responsible for the decay of the ring current during the slow recovery phase of the geomagnetic storm. The probability of charge exchange collisions between the ring current ions and the cold geocorona neutral hydrogen is given in Equation 3.1.

$$\left\langle \frac{\delta Q}{\delta t}_{CE} \right\rangle = -\sigma_{CEi}\sqrt{\frac{2E}{m_i}}\langle n_H \rangle Q \tag{3.1}$$

where σ_{CE_i} is the charge exchange cross section of species i with geocorona H, and $\langle n_H \rangle$ represents the bounced averaged neutral hydrogen density around the equatorial plane. Q, m_i and E are respectively the distribution function, mass of species i and energy of ring current ion species.

Since energetic N^+ and O^+ (> 10 keV) have different charge exchange cross sections, as Figure 2.6 shows, the results will focus more on the slow recovery phase of the geomagnetic storm, which happens approximately from hour 7 to hour 11 of our synthetic geomagnetic storm simulation. Moreover, to fully account for the impact of charge exchange on the loss of the ring current, we apply the Rairden and Hodges geocoronal models in the idealized storm simulation. We examine the importance of N^+ in the inner magnetospheric dynamics from four different perspectives: equatorial pressure, magnetospheric response, decay time of the ring current ions, and authentic TWINS ENA image.

3.1 Equatorial Pressure

Equatorial pressure is a straightforward way to show the change of characteristics in the ring current. The gradient of the ring current equatorial

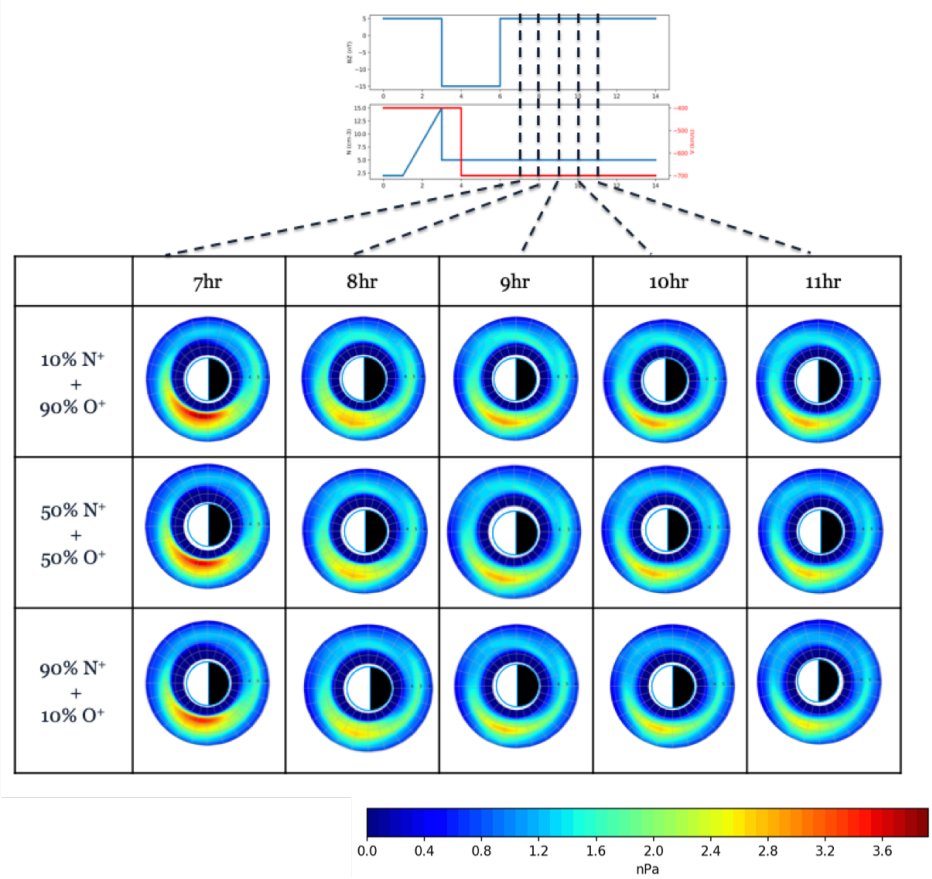

Figure 3.1: Each row represents the equatorial pressure in five snapshots from hour 7 to hour 11 The rows are 10% N^+ with 90% O^+, 50% N^+ with 50% O^+, and 90% N^+ with 10% O^+.

pressure can represent the ring current drift direction. Figure 3.1 shows the total equatorial pressure profile from hour 7 to hour 11, namely during the recovery phase of the synthetic geomagnetic storm. The time of the equatorial pressure profile is indicated by the vertical dashed lines. In order to compare the total equatorial pressure profile with different N^+ concentration, we run three simulations of 10% N^+ with 90% O^+, 50% N^+ with 50% O^+, and 90% N^+ with 10% O^+. For simplicity, these three cases all used the Rairden geocoronal models for neutral H distribution. The pressure profiles shown in Figure 3.1 suggest that the simulation in which we considered 90% N^+ with 10% O^+ can have lower equatorial pressure at the end of hour 11. This tells us that the equatorial pressure for the simulation with higher percentages of N^+ in the ring current during the recovery phase is reduced more than the cases with less N^+ concentration in ring current heavy ions, because N^+ has

larger charge exchange cross section with neutral hydrogen than O^+. Therefore, the N^+ ion is more likely to collide with geocoronal hydrogen atoms, and to become an energetic neutral nitrogen atom. In addition, the topology of the total equatorial pressure profile during the slow recovery phase of the geomagnetic storm changes differently with different N^+ concentrations in the evolution of the ring current. To examine the contribution of N^+ in the ring current evolution, we plot the peak of N^+ and O^+ equatorial pressure in the cases of 10% N^+ with 90% O^+, and 90% N^+ with 10% O^+. From Figure 3.2, we show the peak pressure of N^+ and O^+ in the synthetic simulation. The locations of peak pressure are represented by MLT and L shell. We find that the magnitude of peak pressure of O^+ in the case of 10% N^+ with 90% O^+ is different from that of N^+ in the case of 90% N^+ with 10% O^+, although the peak pressure numbers of minor ion species are very similar. The difference between the peak pressures is remarkable especially during the recovery phase of the geomagnetic storm. Moreover, the locations of peak pressures of N^+ and O^+ in the ring current are not always the same. The peak pressure can happen in different L shell from hour 7 to hour 11 of our simulation storm. These two findings suggest that the presence of N^+ in the ring current can significantly affect the total equatorial pressure profile and therefore the topology of the ring current evolution.

3.2 Decay Time

Figure 3.3 shows the lifetime of ring current ions as a function of pitch angle, energy and L shell, which depends primarily of the charge exchange cross section and the density of neutral hydrogen. For the same ion species, the spatial location of ion species can play a role on the lifetime of ring current ions, since the geocoronal density is exponentially decreasing with distance from the Earth. According to the Figure 3.3, the lifetime of N^+ is at least one order of magnitude shorter than that of O^+. This is because high-energy (>10 keV) N^+ has a larger charge exchange cross section than O^+. Moreover, the pitch angle can also make a large difference. We find that the pitch angle of 30 and 90 can make a difference in decay time of ring current ions. Ring current ions with 30 pitch angle have longer time in the bounce period; therefore, during the long bounce they approach L shells

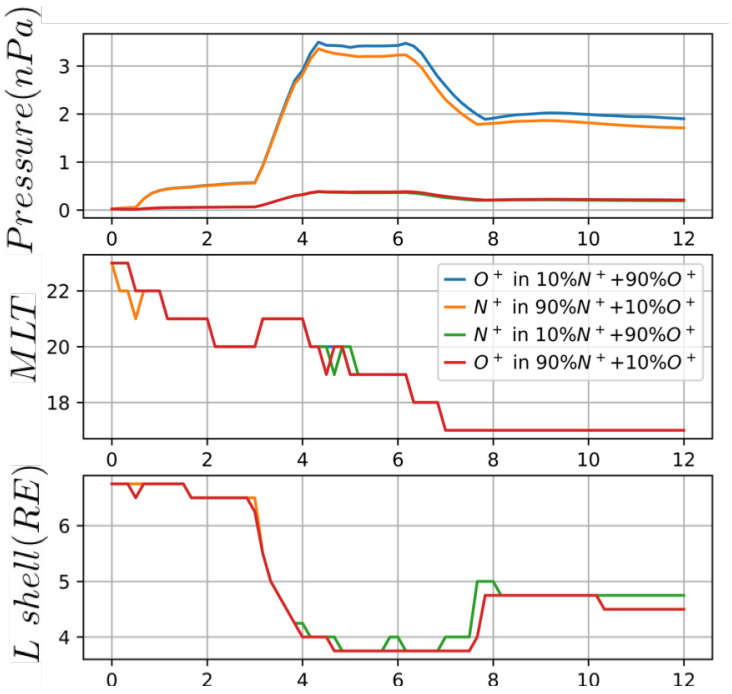

Figure 3.2: The top row is the comparison of peak O^+ pressure and peak N^+ pressure. The other two rows show the location when the peak pressure of N^+ or O^+ happens.

with larger geocoronal densities, and accordingly the probability of charge exchange increases considerably. However, ring current ions with 90 pitch angle only bounce around the mirror point, and thus the decay time is smaller than particles with 30 pitch angle. The decay time of the ring current ions due to charge exchange can determine the loss rate of the ring current ions during the slow recovery phase of the geomagnetic storm. Therefore, the shorter the decay time, the faster the recovery rate of the recovery phase in the geomagnetic storm.

3.3 Magnetospheric Response: Dst (Disturbance Time) Index

The Dst (disturbance time) index represents the intensity of a geomagnetic storm. The Dst is derived by averaging the disturbance of $B_{\|}$ near the Earth's equator. Ilie et al. [11] indicated that for ions less than 100 keV, the decay rate of the ring current varies significantly on the geocoronal density model.

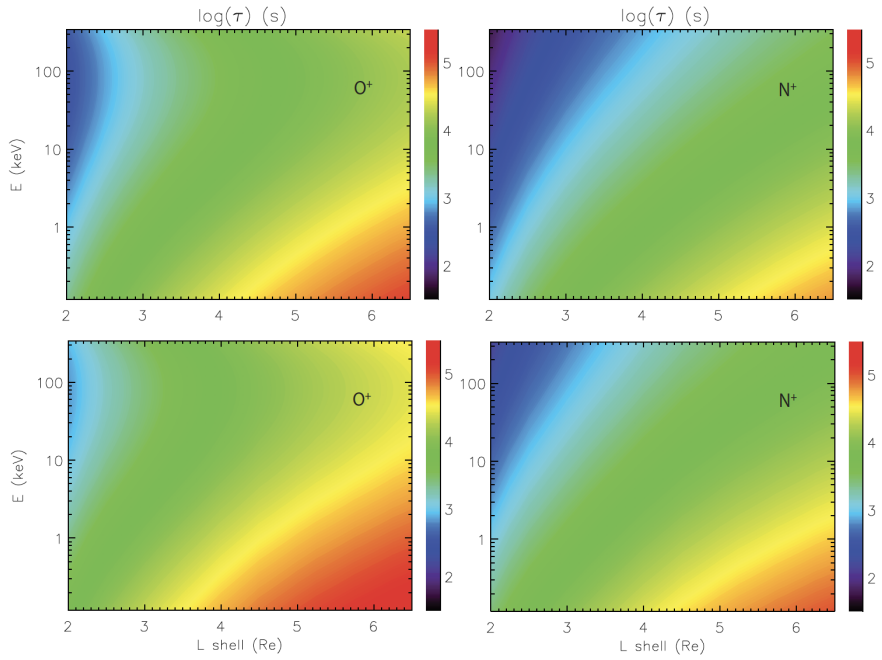

Figure 3.3: The top panels show the bounce averaged lifetimes of O^+ and N^+ as a function of energy and radial distance where pitch angle is 90. The bottom panels show the bounce averaged lifetime where pitch angle is 30.

The difference in charge exchange cross section between N^+ + H and O^+ + H plays a crucial role in the charge exchange reactions, and the impact of N^+ on the ring current with various geocoronal models has remained unknown. Since HEIDI can accommodate six geocoronal models, we use HEIDI to assess the impact of neutral dynamics on ring current development. Figure 3.4 shows the synthetic Dst (representing the magnetospheric response) for simulations involving different N^+/O^+ ratios for the Rairden et al. [47] model (spherically symmetric neutral density distribution) and the Hodges [48] model (predicting a distribution of neutral H with day-night and dawn-dusk asymmetry based on Monte Carlo simulations). We compare six storm simulations with different concentrations of N^+ or geocorona H model. The simulation results suggest that higher concentration of ring current N^+ ions can lead to faster recovery during the slow recovery phase of the geomagnetic storm. In the end of the recovery phase of the geomagnetic storm, the Dst index varies from -50 to -28 (nT). Not only does the Dst index in the end of recovery phase change, but also the depression of the Dst index in the main phase can be affected by the presence of N^+ and different geocoronal hydro-

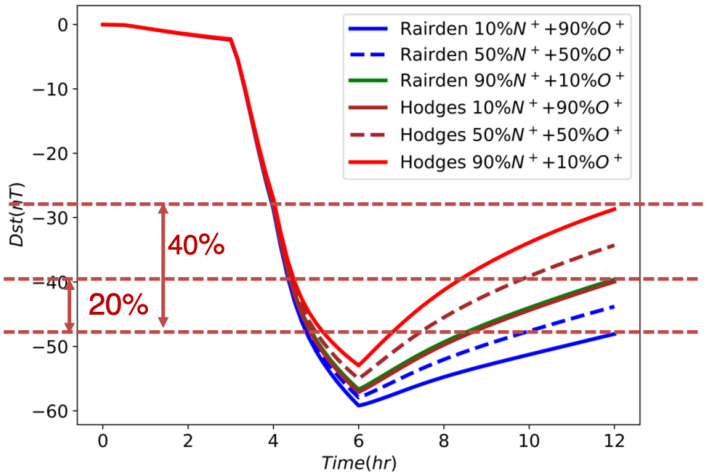

Figure 3.4: Dst vs. time with idealized simulation. Here we run three cases of different N^+ concentration in the ring current heavy ions with Rairden and Hodges geocoronal models.

gen models. These results highlight two points: (1) Due to the difference in charge exchange cross section, higher N^+/O^+ ratio will lead to faster recovery rate in a geomagnetic storm. The difference in recovery rate between high percentage N^+ and low percentage of N^+ can be $\sim 20\%$. (2) The difference in the Dst index produced by using the Rairden et al. [47] vs. the Hodges [48] geocoronal models is $\sim 40\%$ during recovery phase; this is because the Hodges model predicts higher neutral density than the Rairden model. Note that this simulation is based on idealized solar wind condition and a constant ion composition ratio.

3.4 Synthetic TWINS-like ENA Image

Two Wide-angle Imaging Neutral-atom Spectrometers (TWINS) [54] is the first mission to have the ability to image the Earth's three-dimensional magnetosphere from two vantage points. The TWINS can indirectly reconstruct the Earth's inner magnetosphere structure by detecting ENA fluxes, a byproduct of charge exchange reactions of geocorona and ring current. Through detecting ENA fluxes in the inner magnetosphere, the TWINS can derive the distribution of energetic ions in the Earth's ring current. Numer-

ous studies have already used the TWINS ENA images to further understand the inner magnetospheric dynamics [11, 55, 56]. However, the TWINS ENA instrument lacks the capability to separate N^+ from O^+, and thus the composition information of N^+ in the ring ions still remains unknown.

Not only does the presence of N^+ in the ring current ions change the magnetospheric dynamics, but understanding its contribution to the global magnetospheric dynamics will also help interpret the data of space missions. To determine the role of N^+ in proper interpretation of the TWINS data, we generated synthetic TWINS-like ENA images. Synthetic TWINS-like ENA images are constructed as a line-of-sight integration of the simulated ENA fluxes from a specified TWINS position with specific charge exchange cross section of the ring current ions and geocorona H distribution. The equation is provided below:

$$j_{ENA} = \int j_{ion}(l)\sigma_{CE}n_H(l)dl$$

where j_{ion} represents the simulated ring current ion fluxes as calculated by HEIDI, with the same energy range as TWINS data, σ_{CE} is the charge exchange cross section, and n_H is neutral hydrogen density, for which various geocoronal models predict different exosphere distribution.

Figure 3.5 shows the synthetic ENA oxygen image extracted in hour 8 of the simulation, which is during the slow recovery phase of the geomagnetic storm, and can be used to assess how the Earth's magnetospheric structure changes as a result of varying N^+/O^+ ratio. Here we focus on two simulation cases: the ion composition on the outer boundary is set as 100% O^+ in one case, and as 50% N^+ + 50% O^+ in the other. The synthetic O ENA images indicate that the peak ENA oxygen flux of 100% O^+ is 1.64 ($cm^{-2}sr^{-2}s^{-1}keV^{-1}$) while the peak value of 50% N^+ + 50% O^+ is 0.82 ($cm^{-2}sr^{-2}s^{-1}keV^{-1}$) (see Table 3.1). These two ENA oxygen images indicate that when we have 50% N^+ + 50% O^+ in the ring current ions, the true ENA oxygen image should be Figure 3.5 (C).

Moreover, for the simulation with 50% N^+ + 50% O^+, we generated synthetic TWINS O and N ENA images during the storm time. These images show the true O and N ENA fluxes if the TWINS had the ability to distinguish N^+ from O^+ in the inner magnetosphere. As shown in Figure 3.6, we found

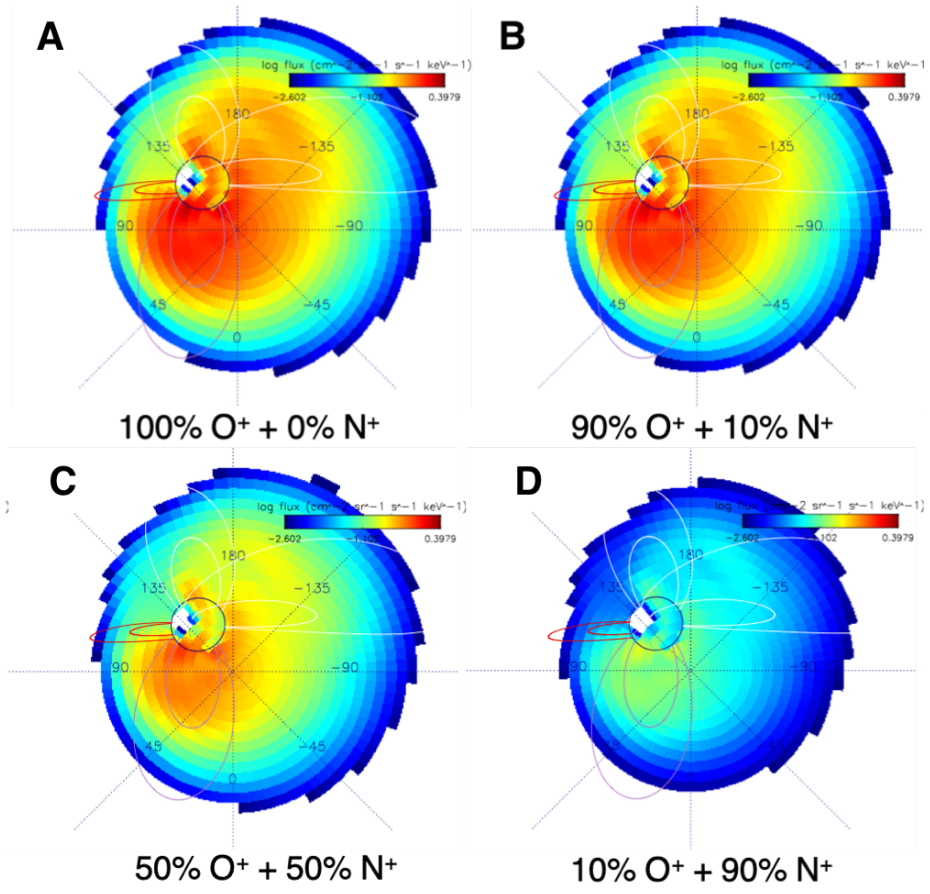

Figure 3.5: Synthetic TWINS oxygen ENA images. Panels A, B, C and D present respectively 100% O^+, 10% N^+ + 90% O^+, 50% N^+ + 50% O^+ and 90% N^+ + 10% O^+.

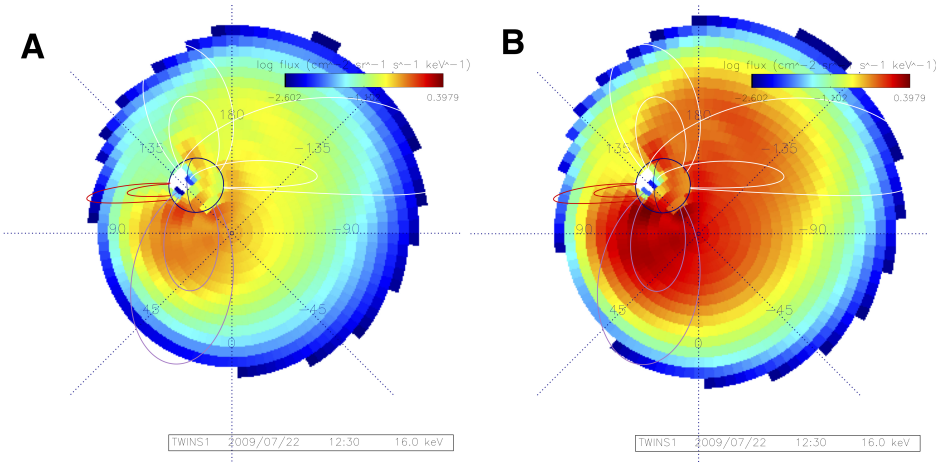

Figure 3.6: Synthetic TWINS oxygen ENA image (A) and nitrogen ENA image (B) for the storm simulation with 50% N^+ + 50% O^+.

Table 3.1: Peak oxygen and nitrogen ENA fluxes for simulations of 100% O^+ and 50% N^+ + 50% O^+. Fluxes are given in $cm^{-2}sr^{-2}s^{-1}keV^{-1}$.

Composition	Oxygen ENA	Nitrogen ENA
0% N^+ + 100% O^+	1.64	0.0
50% N^+ + 50% O^+	0.82	1.39

that the N ENA flux is ∼60% less than the O ENA flux in the simulation with 50% N^+ + 50% O^+.

In reality, since TWINS lacks the ability to separate N^+ from O^+, the TWINS then assumes N^+ as O^+, and thus the TWINS ENA will likely detect oxygen ENA distribution as shown in Figure 3.5 (A). The inaccurate O ENA image may then cause TWINS data to misestimate the concentration of O^+ in the ring current. This suggests that not accounting for the presence of nitrogen ions in the inner magnetosphere can lead to misinterpretation of spacecraft data, as a unity ratio of nitrogen to oxygen can lead to differences in ENA fluxes ($\sim$ 100%).

CHAPTER 4

CONCLUSION AND FUTURE WORK

4.1 Conclusion

The ion compositions in the Earth's magnetosphere and ionosphere have profound influence on magnetospheric dynamics. The mass loading and the topology of the magnetosphere are impacted directly. The wave propagation of the thermal ions in the magnetosphere and the reconnection rates of the dayside magnetosphere are also influenced by the ion compositions in the magnetosphere. Compared with the light ions, heavy ions, such as O^+ and N^+, can strongly affect the magnetospheric dynamics. Studies of O^+ ions have been conducted for a long time, but studies related to the N^+ ions in the Earth's magnetosphere are few. Even though limited, the multiple observations show that the N^+ ions are important in the Earth's magnetosphere and the ionosphere, and O^+ and N^+ ions behave differently during different solar conditions. During the storm time, N^+ ions are constant companions of O^+ on the high-latitude ionosphere from the data of the Akebono satellite. The existence of N^+ in the magnetosphere and ionosphere system can help interpret current magnetospheric data. The Van Allen Probe observed the unexplained fast decay of O^+ in the large L shell. The presence of the fast-decaying N^+ in the magnetospheric plasma might explain such fast decays, since N^+ has a shorter lifetime in the magnetosphere than O^+ due to the different charge exchange cross sections of N^+ and O^+ with geocoronal H.

To understand how the presence of N^+ influences the magnetospheric dynamics, we further developed the HEIDI model to include the behavior of N^+ in the ring current. Although O^+ and N^+ have similar mass and the same charge, they have different properties in the scale height and charge exchange cross section. Charge exchange collisions of ring current ions with

the neutral geocoronal H are the dominant mechanism in the decay of the the ring current during the slow recovery phase of a geomagnetic storm.

The simulation results show a large variation in the slow recovery phase of the geomagnetic storm with the thermal N^+ composition of the ring current. Since N^+ and O^+ have different charge exchange cross sections, different N^+/O^+ ratios in the ring current ion composition lead to changes in the equatorial pressure, decay time of thermal ions and recovery rate in the recovery phase of a geomagnetic storm. Therefore, the concentration of N+ in the ring current can affect the ion equatorial pressure and the magnetic field, causing the variation of the drift velocities and the drift paths of ions in the magnetosphere. In summary, the inclusion of N^+ in the simulation can change the magnetospheric dynamics and the topology of the magnetosphere, especially in the recovery phase of a geomagnetic storm.

The effect of including N^+ also suggests that data from past missions may have been misinterpreted. Since the TWINS lacked the ability to separate N^+ from O^+, it might regard N^+ as O^+ in its observation data. To estimate the possible misinterpretation of the TWINS data, we developed an advanced way to construct the synthetic TWINS-like ENA image based on our simulation results of equatorial number density distribution of thermal ring current ions. The synthetic TWINS-like ENA image can construct what TWINS would see if it could separate N^+ from O^+. The multiple synthetic oxygen and nitrogen ENA images indicate that TWINS might overestimate the concentration of thermal O^+ in the magnetosphere.

Overall, the inclusion of N^+ can change the topology of the magnetosphere, especially during the slow recovery phase of a geomagnetic storm. Due to the the different behaviors of N^+ and O^+ in the inner magnetospheric dynamics, we need to treat N^+ and O^+ as different ion species in the magnetosphere and ionosphere systems. The transport and energization of N^+ from the ionosphere to the magnetosphere through the polar wind are still unknown and further studies are needed.

4.2 Future Work

The ultimate goal of this research is to determine the role of N^+ in the Earth's magnetosphere-ionosphere system. This thesis is just a starting point in the research of N^+. Several research projects are needed in the future. These include studies of (1) how the outcome of including N^+ during the decay of the ring current varies with different geocoronal models, (2) the abundance of N^+ in the ionospheric outflow, and (3) the impact of magnetospheric thermal N^+ on the global magnetospheric dynamics. In the following paragraphs, we expand on each in its turn.

The outcome of including N^+ in the magnetosphere may vary from one applied geocoronal model to another. In this work, we only apply the Rairden and Hodges geocoronal models on a synthetic storm. However, the HEIDI can accommodate six geocoronal models and all of them predict different geocoronal H distribution. We will run a set of idealized and real event simulations under different neutral geocoronal models to determine the impact of different N^+/O^+ ratio on the inner magnetospheric dynamics.

Further development of the ionospheric outflow modeling is required to explore the role of N^+ from the Earth's ionosphere to the magnetosphere. The relative abundance of N^+ in comparison with O^+ in the ionospheric outflow is still in need of study. The transport and acceleration of N^+ in the magnetosphere-ionosphere have remained unknown for a long time. Currently, the Polar Wind Outflow Model (PWOM) only solves the transport equations on the thermal ions of H^+, He^+, O^+, and electrons in the ionospheric outflow. We will expand the PWOM to solve transport equations with N^+ and any related ion species, such as N_2^+, NO^+, and O_2^+, in the polar wind. Though the heavy ions do not easily overcome the Earth's gravity and escape from the ionosphere, the contribution of these heavy ions in the ionospheric outflow cannot be neglected. Including new thermal ion species in the PWOM will change the collision and heat conductivity, and thus the transport solution of ionospheric outflow will be changed completely.

For the role of N^+ in the whole Earth's magnetosphere, we will properly include the contribution of N^+ ions in the magnetospheric models under the

Space Weather Modeling Framework, and assess the role of outflowing N^+ ions in the overall magnetosphere-ionosphere dynamics. As of now, the ion composition in HEIDI is set by the Young's formula [53]. However, in reality, the ion composition in the ring current depends on the ion composition of the global magnetosphere. Coupling the HEIDI with the Block-Adaptive-Tree-Solarwind-Roe-Upwind-Scheme (BATS-R-US) global magnetosphere model can vary the N^+/O^+ ratio on the inner boundary, according to some published research [21, 27, 57–59]. Therefore, we can assess the effect of ion composition variations in the ionosphere as mimicked by the inner boundary of the BATS-R-US model.

REFERENCES

[1] P. Song, H. J. Singer, and G. L. Siscoe, *Space weather*. DC: American Geophysical Union, 2001, vol. 125, ch. 2.

[2] R. Coker, "The trillion-dollar solar storm," *The Space Review*. [Online]. Available: https://www.thespacereview.com/article/3358/1

[3] "Space weather," NASA, n.d. [Online]. Available: https://www.nasa.gov/mission_pages/rbsp/science/rbsp-spaceweather.html

[4] C. J. Schrijver and G. L. Siscoe, *Heliophysics: Plasma physics of the local cosmos*. Cambridge University Press, 2009, ch. 10.

[5] Y. Kamide and A. C.-L. Chian, *Handbook of the Solar-Terrestrial Environment*. Springer Science & Business Media, 2007.

[6] "Earth's magnetosphere and plasmasheet," NASA, n.d. [Online]. Available: https://www.nasa.gov/mission_pages/sunearth/science/magneto-sphere2.html

[7] N. Y. Ganushkina, M. Liemohn, and S. Dubyagin, "Current systems in the earth's magnetosphere," *Reviews of Geophysics*, vol. 56, no. 2, pp. 309–332, 2018.

[8] B. T. Tsurutani and W. D. Gonzalez, "The cause of high-intensity long-duration continuous AE activity (HILDCAAS) - Interplanetary Alfven wave trains," *Planetary Space Science*, vol. 35, pp. 405–412, Apr. 1987.

[9] I. A. Daglis, R. M. Thorne, W. Baumjohann, and S. Orsini, "The terrestrial ring current: Origin, formation, and decay," *Reviews of Geophysics*, vol. 37, pp. 407–438, 1999.

[10] T. I. Gombosi, *Physics of the Space Environment*. Cambridge University Press, 1998, ch. 1.

[11] R. Ilie, R. M. Skoug, H. O. Funsten, M. W. Liemohn, J. J. Bailey, and M. Gruntman, "The impact of geocoronal density on ring current development," *Journal of Atmospheric and Solar-Terrestrial Physics*, vol. 99, pp. 92–103, July 2013.

[12] M. W. Liemohn, J. U. Kozyra, V. K. Jordanova, G. V. Khazanov, M. F. Thomsen, and T. E. Cayton, "Analysis of early phase ring current recovery mechanisms during geomagnetic storms," *Geophysical Research Letters*, vol. 26, pp. 2845–2848, Sep. 1999.

[13] J. U. Kozyra, M. W. Liemohn, C. R. Clauer, A. J. Ridley, M. F. Thomsen, J. E. Borovsky, J. L. Roeder, V. K. Jordanova, and W. D. Gonzalez, "Multistep Dst development and ring current composition changes during the 4-6 June 1991 magnetic storm," *Journal of Geophysical Research (Space Physics)*, vol. 107, p. 1224, Aug. 2002.

[14] M. Fok, J. U. Kozyra, A. F. Nagy, C. E. Rasmussen, and G. V. Khazanov, "Decay of equatorial ring current ions and associated aeronomical consequences," *Journal of Geophysical Research*, vol. 98, pp. 19 381–19 393, Nov. 1993.

[15] Y. I. Feldstein, A. E. Levitin, S. A. Golyshev, L. A. Dremukhina, U. B. Vestchezerova, T. E. Valchuk, and A. Grafe, "Ring current and auroral electrojets in connection with interplanetary medium parameters during magnetic storm," *Annales Geophysicae*, vol. 12, pp. 602–611, Aug. 1994.

[16] D. C. Hamilton, G. Gloeckler, F. M. Ipavich, B. Wilken, and W. Stuedemann, "Ring current development during the great geomagnetic storm of February 1986," *Journal of Geophysical Research*, vol. 93, pp. 14 343–14 355, Dec. 1988.

[17] R. M. Winglee, D. Chua, M. Brittnacher, G. K. Parks, and G. Lu, "Global impact of ionospheric outflows on the dynamics of the magnetosphere and cross-polar cap potential," *Journal of Geophysical Research (Space Physics)*, vol. 107, p. 1237, Sep. 2002.

[18] G. Gloeckler, F. M. Ipavich, B. Wilken, W. Stuedemann, and D. Hovestadt, "First composition measurement of the bulk of the storm-time ring current (1 to 300 keV/e) with AMPTE-CCE," *Geophysical Research Letters*, vol. 12, pp. 325–328, May 1985.

[19] U. Mall, S. Christon, E. Kirsch, and G. Gloeckler, "On the solar cycle dependence of the N^+/O^+ content in the magnetosphere and its relation to atomic N and O in the Earth's exosphere," *Geophysical Research Letters*, vol. 29, no. 1, pp. 34–1, June 2002.

[20] E. G. Shelley, R. G. Johnson, and R. D. Sharp, "Satellite observations of energetic heavy ions during a geomagnetic storm," *Journal of Geophysical Research*, vol. 77, p. 6104, 1972.

[21] R. W. Schunk and W. J. Raitt, "Atomic nitrogen and oxygen ions in the daytime high-latitude F-region," *Journal of Geophysical Research(Space Physics)*, vol. 85, pp. 1255–1272, 1980.

[22] R. W. Schunk and J. J. Sojka, "Global ionosphere-polar wind system during changing magnetic activity," *Journal of Geophysical Research*, vol. 102, no. A, pp. 11 625–11 652, June 1997.

[23] M. Nosé, S. Taguchi, K. Hosokawa, S. P. Christon, R. W. McEntire, T. E. Moore, and M. R. Collier, "Overwhelming O^+ contribution to the plasma sheet energy density during the October 2003 superstorm: Geotail/EPIC and IMAGE/LENA observations," *Journal of Geophysical Research(Space Physics)*, vol. 110, no. A, Sep. 2005.

[24] A. R. Barakat and R. W. Schunk, "A three-dimensional model of the generalized polar wind," *Journal of Geophysical Research (Space Physics)*, vol. 111, no. A, p. A12314, Dec. 2006.

[25] A. Glocer, G. Tóth, T. Gombosi, and D. Welling, "Modeling ionospheric outflows and their impact on the magnetosphere, initial results," *Journal of Geophysical Research (Space Physics)*, vol. 114, no. A13, p. 5216, May 2009.

[26] A. Glocer, N. Kitamura, G. Toth, and T. Gombosi, "Modeling solar zenith angle effects on the polar wind," *Journal of Geophysical Research (Space Physics)*, vol. 117, no. A16, p. 4318, Apr. 2012.

[27] J. H. Hoffman, W. H. Dodson, C. R. Lippincott, and H. D. Hammack, "Initial ion composition results from the Isis 2 satellite," *Journal of Geophysical Research*, vol. 79, pp. 4246–4251, Oct. 1974.

[28] C. R. Chappell, S. A. Fields, C. R. Baugher, J. H. Hoffman, W. B. Hanson, W. W. Wright, H. D. Hammack, G. R. Carignan, and A. F. Nagy, "The retarding ion mass spectrometer on Dynamics Explorer-A," *Space Science Instrumentation*, vol. 5, pp. 477–491, Dec. 1981.

[29] P. D. Craven, R. H. Comfort, P. G. Richards, and J. M. Grebowsky, "Comparisons of modeled N^+, O^+, H^+, and He^+ in the midlatitude ionosphere with mean densities and temperatures from Atmosphere Explorer," *Journal of Geophysical Research (Space Physics)*, vol. 100, no. A1, pp. 257–268, Jan. 1995.

[30] B. A. Whalen, J. R. Burrows, A. W. Yau, E. E. Budzinski, A. M. Pilon, I. Iwamoto, K. Marubashi, S. Watanabe, H. Mori, and E. Sagawa, "The suprathermal ion mass spectrometer (SMS) onboard the Akebono (EXOS-D) satellite," *Journal of Geomagnetism and Geoelectricity*, vol. 42, no. 4, pp. 511–536, 1990.

[31] A. Yau and B. Whalen, "Auroral ion composition during large magnetic storms," *Canadian Journal of Physics*, vol. 70, no. 7, pp. 500–509, 1992.

[32] A. W. Yau, B. A. Whalen, and E. Sagawa, "Minor ion composition in the polar ionosphere," *Geophysical Research Letters*, vol. 18, no. 2, pp. 345–348, Feb. 1991.

[33] M. Bashir and R. Ilie, "A new N^+ band of electromagnetic ion cyclotron waves in multi-ion cold plasmas," *Geophysical Research Letters*, vol. 45, no. 19, pp. 10–150, 2018.

[34] A. Gerrard, L. Lanzerotti, M. Gkioulidou, D. Mitchell, J. Manweiler, J. Bortnik, and K. Keika, "Initial measurements of O-ion and He-ion decay rates observed from the Van Allen probes RBSPICE instrument," *Journal of Geophysical Research(Space Physics)*, vol. 119, no. 11, pp. 8813–8819, Nov. 2014.

[35] R. Ilie, M. W. Liemohn, G. Toth, N. Yu Ganushkina, and L. K. S. Daldorff, "Assessing the role of oxygen on ring current formation and evolution through numerical experiments," *Journal of Geophysical Research (Space Physics)*, vol. 120, no. 6, pp. 4656–4668, 2015, 2015JA021157. [Online]. Available: http://dx.doi.org/10.1002/2015JA021157

[36] W. D. Gonzalez, J. A. Joselyn, Y. Kamide, H. W. Kroehl, G. Rostoker, B. T. Tsurutani, and V. M. Vasyliunas, "What is a geomagnetic storm?" *Journal of Geophysical Research*, vol. 99, pp. 5771–5792, Apr. 1994.

[37] A. T. Y. Lui, "Inner magnetospheric plasma pressure distribution and its local time asymmetry," *Geophysical Research Letters*, vol. 30, no. 16, pp. 160 000–1, Aug. 2003.

[38] A. M. Jorgensen, H. E. Spence, W. J. Hughes, and H. J. Singer, "A statistical study of the global structure of the ring current," *Journal of Geophysical Research (Space Physics)*, vol. 109, no. A18, p. 12204, Dec. 2004.

[39] M. W. Liemohn, "Yet another caveat to using the Dessler-Parker-Sckopke relation," *Journal of Geophysical Research*, vol. 108, no. A6, p. 1251, 2003, 1251. [Online]. Available: http://dx.doi.org/10.1029/2003JA009839

[40] V. K. Jordanova, S. Zaharia, and D. T. Welling, "Comparative study of ring current development using empirical, dipolar, and self-consistent magnetic field simulations," *Journal of Geophysical Research(Space Physics)*, vol. 115, no. A, Dec. 2010.

[41] F. Toffoletto, S. Sazykin, R. Spiro, and R. Wolf, "Inner magnetospheric modeling with the Rice Convection Model," *Space Science Reviews*, vol. 107, pp. 175–196, Apr. 2003.

[42] N. Y. Ganushkina, M. W. Liemohn, M. V. Kubyshkina, R. Ilie, and H. J. Singer, "Distortions of the magnetic field by storm-time current systems in Earth's magnetosphere," *Annales Geophysicae*, vol. 28, pp. 123–140, Jan. 2010.

[43] R. Ilie, M. W. Liemohn, G. Toth, and R. M. Skoug, "Kinetic model of the inner magnetosphere with arbitrary magnetic field," *Journal of Geophysical Research (Space Physics)*, vol. 117, p. 4208, Apr. 2012.

[44] H. Volland, "A semiempirical model of large-scale magnetospheric electric fields," *Journal of Geophysical Research*, vol. 78, p. 171, 1973.

[45] D. P. Stern, "The motion of a proton in the equatorial magnetosphere," *Journal of Geophysical Research*, vol. 80, p. 595, 1975.

[46] N. C. Maynard and A. J. Chen, "Isolated cold plasma regions - Observations and their relation to possible production mechanisms," *Journal of Geophysical Research*, vol. 80, pp. 1009–1013, Mar. 1975.

[47] R. L. Rairden, L. A. Frank, and J. D. Craven, "Geocoronal imaging with Dynamics Explorer," *Journal of Geophysical Research*, vol. 91, pp. 13 613–13 630, Dec. 1986.

[48] R. R. Hodges, Jr., "Monte Carlo simulation of the terrestrial hydrogen exosphere," *Journal of Geophysical Research*, vol. 99, pp. 23 229–23 247, Dec. 1994.

[49] N. Østgaard, S. B. Mende, H. U. Frey, G. R. Gladstone, and H. Lauche, "Neutral hydrogen density profiles derived from geocoronal imaging," *Journal of Geophysical Research (Space Physics)*, vol. 108, p. 1300, July 2003.

[50] J. H. Zoennchen, J. J. Bailey, U. Nass, M. Gruntman, H. J. Fahr, and J. Goldstein, "3-D-geocoronal hydrogen density derived from TWINS Ly-α-data," *Annales Geophysicae*, vol. 13, July 2011.

[51] J. Bailey and M. Gruntman, "Experimental study of exospheric hydrogen atom distributions by Lyman-alpha detectors on the TWINS mission," *Journal of Geophysical Research (Space Physics)*, vol. 116, no. A15, p. A09302, Sep. 2011.

[52] J. Bailey and M. Gruntman, "Experimental study of the asymmetric time varying exosphere by Lyman-alpha detectors on the TWINS mission," *European Planetary Science Congress*, vol. 8, p. 861, Sep. 2013.

[53] D. T. Young, H. Balsiger, and J. Geiss, "Correlations of magnetospheric ion composition with geomagnetic and solar activity," *Journal of Geophysical Research*, vol. 87, pp. 9077–9096, Nov. 1982.

[54] D. J. McComas, F. Allegrini, J. Baldonado, B. Blake, P. C. Brandt, J. Burch, J. Clemmons, W. Crain, D. Delapp, R. Demajistre, D. Everett, H. Fahr, L. Friesen, H. Funsten, J. Goldstein, M. Gruntman, R. Harbaugh, R. Harper, H. Henkel, C. Holmlund, G. Lay, D. Mabry, D. Mitchell, U. Nass, C. Pollock, S. Pope, M. Reno, S. Ritzau, E. Roelof, E. Scime, M. Sivjee, R. Skoug, T. S. Sotirelis, M. Thomsen, C. Urdiales, P. Valek, K. Viherkanto, S. Weidner, T. Ylikorpi, M. Young, and J. Zoennchen, "The two wide-angle imaging neutral-atom spectrometers (TWINS) NASA mission-of-opportunity," *Space Science Review*, vol. 142, pp. 157–231, Feb. 2009.

[55] N. Buzulukova, M. C. Fok, A. Pulkkinen, M. Kuznetsova, T. E. Moore, A. Glocer, Brandt, P. C., G. Tóth, and L. Rastätter, "Dynamics of ring current and electric fields in the inner magnetosphere during disturbed periods: CRCM-BATS-R-US coupled model," *Journal of Geophysical Research*, vol. 115, no. A, p. A05210, May 2010.

[56] P. Valek, P. C. Brandt, N. Buzulukova, M.-C. Fok, J. Goldstein, D. J. McComas, J. D. Perez, E. Roelof, and R. Skoug, "Evolution of low-altitude and ring current ENA emissions from a moderate magnetospheric storm: Continuous and simultaneous TWINS observations," *Journal of Geophysical Research (Space Physics)*, vol. 115, no. A14, p. A11209, Nov. 2010.

[57] H. A. J. Taylor, H. C. Brinton, M. W. I. Pharo, and N. K. Rahman, "Thermal ions in the exosphere: evidence of solar and geomagnetic control," *Journal of Geophysical Research*, vol. 73, no. 1, pp. 5521–5533, Sep. 1968.

[58] H. C. Brinton, J. M. Grebowsky, and H. G. Mayr, "Altitude variation of ion composition in midlatitude trough region: Evidence for upward plasma flow," *Journal of Geophysical Research (Space Physics)*, vol. 76, no. 16, pp. 3738–3745, 1971.

[59] J. J. Sojka, R. W. Schunk, and W. J. Raitt, "Seasonal-variations of the high-latitude F-region for strong convection," *Journal of Geophysical Research (Space Physics)*, vol. 87, no. NA1, pp. 187–198, 1982.